Theoretical Attempts to Optimize the Geometrical Shape of Simple Electromagnetic Rail Launcher

Shaohui Chen[1,2(✉)] and Hongyan Sun[2]

[1] Institute Electrical Engineering, Chinese Academy of Sciences, Beijing 100190, China
shaohui818@163.com
[2] Beijing Aeronautical Technology Research Center, Beijing 100076, China

Abstract. Inductance gradient, an important parameter that affects the performance of electromagnetic rail launcher, is mainly determined by the geometrical shape of the launcher. This study therefore intends to analyze the influence of the rail's height and width on the inductance gradient, with the area of the cross-section of the guiding rail fixed. The study finds that the maximum inductance gradient peaks when the guiding rail section is rectangular (i.e., its width is greater than height) under both the high- and low-frequency circumstances. Attempts are also made to establish arithmetic models for forcing and masses of the launch load with a pulsed current. The optimum rail separation is thereupon derived at high- and low-frequency, respectively, to maximize the initial velocity of the effective payload. The results show that the rectangular aperture launcher with rail separation greater than rail height can maximize the initial velocity of payload.

Keywords: Inductance gradient · Electromagnetic rail launcher · Geometrical shape · Optimization

1 Introduction

Electromagnetic railgun is a new technology that uses extremely high ampere force generated by pulsed large current flows through the rails and armature to accelerate the armature and payload to thousands of meters per second in milliseconds. It boasts of high initial speed, high cost-effectiveness ratio, high security, good controllability and good concealment, harbors great application potential in various fields ranging from military, aerospace to scientific experiment and hence draws wide attention and support from various countries [1–4].

Factors of the electromagnetic rail launcher such as its structure, size, section shape, and material are directly related to its inductance gradient value (i.e., the inductance value of the per unit length rail), which ultimately determines the force on the armature and affects both the muzzle kinetic energy and launch efficiency. The inductance gradient value of the launcher is therefore one of the most important research fields in

X. Liang et al. (Eds.): *The proceedings of the 16th Annual Conference of China Electrotechnical Society*, LNEE 890, pp. 12–23, 2022.
https://doi.org/10.1007/978-981-19-1870-4_2

the electromagnetic rail launch technology, and is mainly approached by analytical or numerical method.

Kerrisk [5] studied the case when the magnetic field does not diffuse into the rail and the current is mainly concentrated on the surface of the rail, and gave the analytical formula for high-frequency inductance gradient. Grover et al. [6] studied the case when the magnetic field diffuses into the rail and the current diffuses completely in the rail, and gave the formula for low-frequency inductance gradient under steady state. Batteh et al. [7] proposed an analytical algorithm for inductance gradient of plasma armature electromagnetic rail launcher, which ignores the influence of rail thickness and current diffusion. Based on the skin effect and magnetic energy equivalence principle, Peng Zhiran et al. [8] proposed an analytical expression of inductance gradient considering the influence of both rail size and current diffusion.

Xu Rong et al. [9] studied the influence factors of electromagnetic field distribution and inductance gradient of augmented railgun using finite element simulation method; Sun Liqiang et al. [10] used the modeling and simulation method to obtain the rail inductance gradient corresponding to different times in the actual electromagnetic launch process; Ghassemi et al. [11] obtained the inductance gradient versus time curve under a given current through transient field simulation. Keshtka et al. [12, 13] designed the armature and rail model through the finite element software, considered the existence of armature in the inductance gradient analysis, and analyzed the relationship between the rail thickness and width and the inductance gradient. Finally, it is concluded that the inductance gradient is greatly affected by the separation, and the inductance gradient increases gradually with the increase of the separation. Li Xiaojiang et al. [14] analyzed the influence of the change of rail geometry on armature muzzle velocity and muzzle kinetic energy, and thereupon optimized the rail geometry using genetic algorithm with armature muzzle kinetic energy as the objective function. Wang Zhizeng et al. [15] derived the expression of inductance gradient under two-dimensional transient condition from the perspective of magnetic energy, and obtained the diffusion behavior of electromagnetic field in rail through solving the magnetic field control expression.

The aforementioned studies have deepened our understanding of inductance gradient in both theoretical and numerical simulation approaches. But their efforts to optimize the geometric dimension of electromagnetic rail launcher were not geared to maximize the initial velocity of effective payload consisting of armature and payload. This study aims to maximize the initial velocity of payload through the construction of a mathematical model of launch load force and mass based on inductance gradient theory, and hence to optimize the geometric size of electromagnetic rail launcher.

2 Inductance Gradient Theory

The theoretical calculation of inductance gradient of rails can be categorized into high- and low-frequency cases.

2.1 High-Frequency Inductance Gradient

High-frequency inductance gradient refers to cases when the magnetic field cannot diffuse to the depth of the rail but only flow along the surface of the rail. Kerrisk calculated

the current distribution in the rectangular rail of the square aperture rail launcher, and proposed an algebraic method to calculate the high-frequency inductance gradient (as shown in Fig. 1), which is known as "Kerrisk L" (unit is $\mu H/m$) [5]:

$$L^{'} = [A + B\ln(F_1)]\ln(F_2) \tag{1}$$

Where:

$$F_1 = 1 + A_1(w/h) + A_2(w/h)(s/h)$$

$$F_2 = B_1 + B_2(s/h) + B_3(w/h) + B_4(s/h)(w/h)$$

$$\begin{aligned} A &= 0.4406 \\ B &= -0.0777 \\ A_1 &= 3.397 \\ A_2 &= -0.06603 \\ B_1 &= 1.0077 \\ B_2 &= 2.7437 \\ B_3 &= 0.02209 \\ B_4 &= 0.2637 \end{aligned}$$

w is the rail width, h is the rail height, and s is the separation.

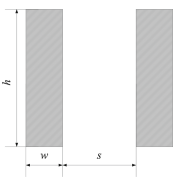

Fig. 1. Rails' cross-section: h-height, w-width, and s-separation.

2.2 Low-Frequency Inductance Gradient

When the current density is evenly distributed in the rail, the inductance gradient can be considered of low-frequency. Grover proposed a simple algebraic method to calculate the low-frequency inductance gradient of the rectangular rail (see Fig. 1), as is shown below (unit is $\mu H/m$) [6]:

$$L^{'} = 0.4\left[\ln\left(\frac{s+w}{h+w}\right) + 1.5 + \ln(k)\right] \tag{2}$$

where $\ln(k)$ is obtained by looking up the table according to s/h and w/h.

2.3 Influence of the Tail Section Size on Inductance Gradient

From formulas (1) and (2), the main factors affecting the inductance gradient of rectangular rail are the rail width, height and separation, in which the rail width and height determine the cross-sectional area of rail and basically determine the carrying capacity of rail. This paper assumes that the cross-sectional area of the rail is a fixed value of 450 mm^2, with the height of the rail varying between 5 mm–30 mm and the width between 90 mm–15 mm.

Figures 2, 3 and 4 show the variation of high- and low-frequency inductance gradients with, respectively, rail height, width and w/h ratio when the separation is 30 mm. Both high- and low-frequency inductance gradients show increases followed by decreases with increasing rail height and width, though at different variation amplitudes. When the maximum of high-frequency inductance gradient is 0.5845 μH the height and width of the rail are 10.9 mm and 41.3 mm respectively, and the w/h value is 3.79. While when the maximum of low-frequency inductance gradient is 0.7274 μH the height and width of the rail are 11 mm and 40.9 mm respectively, and the w/h value is 3.72. It can be seen that under the assumption that the rail cross-sectional area is a fixed value, the inductance gradient is large when the rail cross-section is rectangular (i.e., width is greater than height). The differences are small in the rail height, width and w/h ratio between maximum high- and low-frequency inductance gradients. In other words, no significant differences exist for the inductance gradient calculations from the design point of view, be it of high- or low-frequency cases.

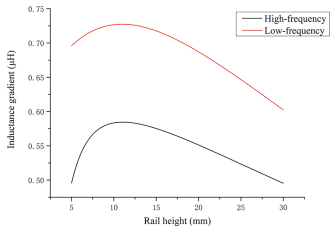

Fig. 2. Variation of the inductance gradient with the rail height

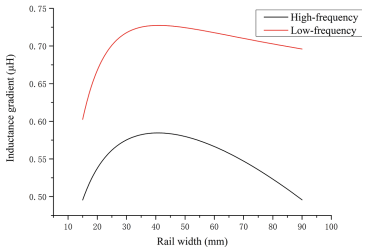

Fig. 3. Variation of the inductance gradient with the rail width

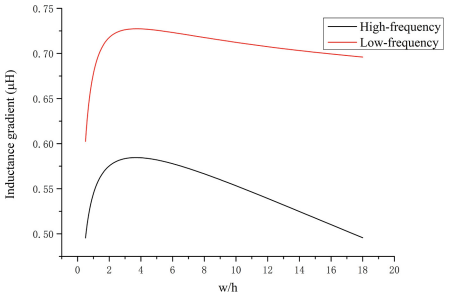

Fig. 4. Variation of the inductance gradient with w/h

2.4 Influence of Separation on Inductance Gradient

Figure 5 shows the variation of high- and low-frequency inductance gradient with separation when the rail height is set at 11 mm and the width 40.9 mm. The variation trend of high-frequency and low-frequency inductance gradient with separation is basically the same. The inductance gradient increases with the increase in the separation. The inductance gradient increases faster when the separation is narrow than wide separation.

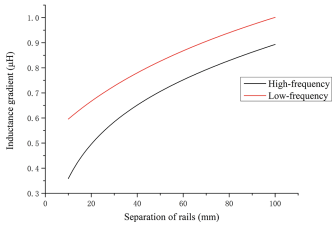

Fig. 5. Variation of the inductance gradient with the separation of the rails

3 Mathematical Model of Launch Load

The electromagnetic rail launch requires the electromagnetic force on the launch load to be directly proportional to the inductance gradient and square of the current. As the electromagnetic thrust increases with inductance gradient under the equivalent current waveform, the widening in the separation will lead to increase in the effective inductance gradient. For the electromagnetic rail launcher, however, the widening in the separation also leads to increases in the volume and mass of the launch load consisting of effective payload and armature, and hence may not always result in a maximum muzzle velocity of the payload. Separation A mathematical model considering both forcing and the mass of the launch load is therefore needed for the optimal separation to achieve the maximum muzzle velocity of payload.

3.1 Mathematical Model of Forcing on the Launch Load

A schematic map of the armature structure is shown in Fig. 6, and its force-bearing scenario is shown in Fig. 7, having ignored the air resistance, viscous resistance, ablation resistance and other factors and highlighted the effect on the armature by the electromagnetic force, rail pressure and friction. The payload is hence mainly affected by the thrust of armature and the friction of rail.

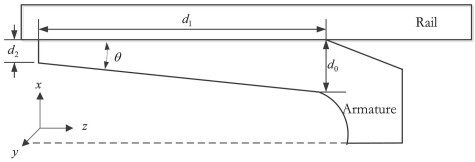

Fig. 6. The armature diagram

In Fig. 6, d0 represents the tail root thickness, d_1 the tail length, d_2 the tail end thickness, and θ the inclination angle of the tail wing. The constraint relationship between the parameters is:

$$d_0 = d_2 + d_1 \tan\theta \tag{3}$$

Among them, the electromagnetic force F acting on the side tail of the armature is given by (4):

$$F = \frac{L'I^2}{2} \cdot \frac{d_1}{X} \tag{4}$$

Where X is the armature width in the x direction, with its value equivalent to the separation s.

In Fig. 7, the tail wing on one side of the armature is subjected to the mechanical interference, $F_{C,}$ electromagnetic component, $F\cos\theta$, and tail pressure on the rail in the x direction, $F_{r,}$ all three summing up to zero if we assume no relative movement of the rail and armature tail in the direction during the launch.

In the z direction, otherwise, the tail wings on both sides of the armature are subjected to friction, $2f_1$, while the armature head is subjected to electromagnetic force, $L'I^2/2$. Meanwhile, the two sides of the payload are subjected to friction $2f_2$. The combination of all three forces result in the acceleration of the launch load along the z direction.

The friction force on one side of the armature tail can be determined by applying Eq. (4) as follows:

$$\begin{aligned} f_1 &= \mu_1(F_C + F\cos\theta) \\ &= \mu_1\left(F_C + \frac{L'I^2 d_1}{2X}\cos\theta\right) \end{aligned} \tag{5}$$

where μ_1 is the dynamic friction coefficient.

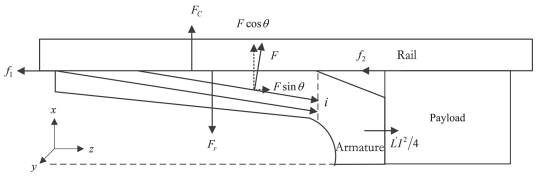

Fig. 7. Cross section of the launch load

Considering $X = s$, the resultant force of launch load in the z direction is:

$$\begin{aligned} F_A &= \frac{L^{'}I^2}{2} - 2f_1 - 2f_2 \\ &= \frac{L^{'}I^2}{2} - 2\mu_1\left(F_C + \frac{L^{'}I^2 d_1}{2X}\cos\theta\right) - 2f_2 \\ &= L^{'}I^2\left(\frac{1}{2} - \frac{\mu_1 d_1}{s}\cos\theta\right) - 2(\mu_1 F_C + f_2) \end{aligned} \tag{6}$$

in which the friction force $2f_2$ on the payload is assumed to be a fixed value.

3.2 Mathematical Model of Launch Load Mass

The launch load is composed of payload and armature. The mass and muzzle velocity of the payload are generally determined by the launch mission. It can be assumed that its mass does not change with the calibre. The armature mass is mainly composed of the mass of the tail wings on both sides and that of the head (Fig. 8). The armature tail wings are mainly used to ensure good contact between the armature and the rail, channel the current on the rail into the armature, or into the rail. It can be considered that its mass does not change with the separation, but changes in proportion with the height of the rail. Driven by the electromagnetic force, the armature head directly accelerates the movement of the effective payload. The payload mass thus not only has a certain structural strength, but also carries the expected current, hence is expressed as follows:

$$\begin{aligned} M &= m_0 + m_a \\ &= m_0 + 2m_{tail} + m_{top} \\ &= m_0 + 2\tau(h - 2\Delta h) + \rho sc(h - 2\Delta h) \end{aligned} \tag{7}$$

Where, m_0 is the payload mass, m_{tail} the mass of the armature tail on one side, m_{top} the mass of the armature head, τ is a constant, $h - 2\Delta h$ the armature height, Δh the gap between one side of the armature and the insulating support, ρ the armature material density, s the separation, and c the armature head thickness.

4 Discussion on the Optimal Separation

In the process of electromagnetic rail launch, the payload, consisting of the payload and armature, accelerates as a whole with the armature thrust. The payload, armature and

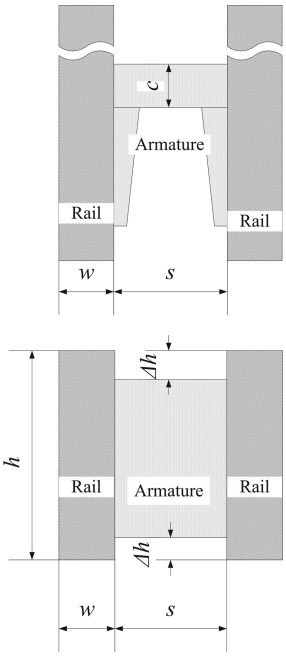

Fig. 8. Bird's view of the armature and rails

launch load have the same speed and acceleration, with the speed expressed as:

$$v = \int a dt = \int \frac{F_A}{M} dt \tag{8}$$

The separation corresponding to the maximum speed can be obtained by equating the derivative of s in formula (8) to zero. That is:

$$\begin{aligned} &\frac{\partial v}{\partial s} = \int \frac{\partial\left(\frac{F_A}{M}\right)}{\partial s} dt = 0 \\ &\Rightarrow \frac{\partial\left(\frac{F_A}{M}\right)}{\partial s} = 0 \end{aligned} \tag{9}$$

4.1 The Optimal Separation at High-Frequency

The payload acceleration at high-frequency can be obtained from Eqs. (1), (6) and (7):

$$\begin{aligned} a_h &= \frac{F_A}{M} \\ &= \frac{[A + B\ln(F_1)]\ln(F_2) I^2\left(\frac{1}{2} - \frac{\mu_1 d_1}{s}\cos\theta\right)}{m_0 + 2\tau(h - 2\Delta h) + \rho sc(h - 2\Delta h)} - \\ &\frac{2(\mu_1 F_C + f_2)}{m_0 + 2\tau(h - 2\Delta h) + \rho sc(h - 2\Delta h)} \end{aligned} \tag{10}$$

The optimum separation can be obtained by calculating the derivative of the rails' (s) and equating it to zero at high-frequency:

$$\frac{[A + B\ln(F_1)]\ln(F_2)I^2K}{M^2} - \frac{2\rho c(\mu_1 F_C + f_2)(h - 2\Delta h)}{M^2} = 0 \tag{11}$$

Where,

$$K = \frac{\mu_1 d_1 M\cos\theta}{s^2} - \frac{\rho c(h - 2\Delta h)}{2} + \frac{\mu_1 d_1 \rho c(h - 2\Delta h)\cos\theta}{s}$$

$$M = m_0 + 2\tau(h - 2\Delta h) + \rho sc(h - 2\Delta h)$$

The application of the equation can be exemplified by a specific case. Suppose the discharge current is a pulsed current (Fig. 9) with the peak value being 200 kA, and the current rising and falling at, respectively, 4×10^8 and -8×10^7A/s. Other input parameters are set as below, with the sectional area of the rail as 450 mm^2, the kinetic friction coefficient 0.04, the length and inclination angle of the tail wing 16 mm and 0.23 rad, respectively, the interference pressure of the armature 1000 N, the friction force on one side of the payload 100 N, the armature head 5.5 mm in thickness, the spacing between the armature and the insulating support as 2 mm, the payload mass as 12g, τ 0.167 g/mm, and the density of the aluminum armature material as 2.7×10^{-3} g/mm^3.

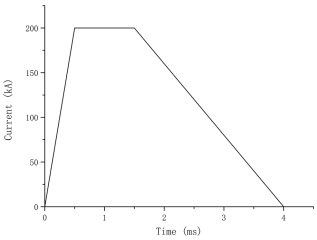

Fig. 9. Variation of the current with time at high-frequency

In the aforementioned case, the variations of the muzzle velocity and separation are studied under five different conditions, i.e., muzzle separation when the rail height is 14 mm, 18 mm, 22 mm, 26 mm and 30 mm, respectively (Fig. 10). Correspondingly, the maximum muzzle velocity is 1181.97 m/s, 973.50 m/s, 817.04 m/s, 695.78 m/s and 599.69 m/s respectively, the separation 66mm, 60mm, 57mm, 55mm and 55 mm respectively, and the corresponding launch load mass 25.14 g, 29.15 g, 33.25 g and 37.32 g and 41.92 g, respectively. Hence the optimal separation decreases with the increase in the rail height, and the separation is always greater than the rail height. This implies that, the muzzle velocity is the largest when generated by a launcher of rectangular calibre.

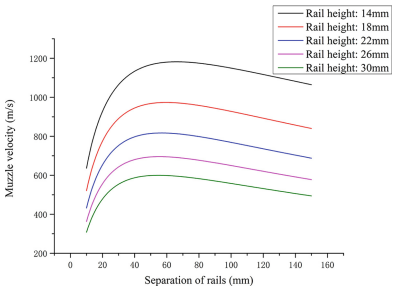

Fig. 10. Variation of the muzzle velocity with the separation and height of rails at high-frequency

4.2 The Optimal Separation at Low-Frequency

The acceleration of the launch load at low-frequency can be yielded from Eqs. (2), (6) and (7) as follows:

$$\begin{aligned} a_l &= \frac{F_A}{M} \\ &= \frac{0.4\left[\ln\left(\frac{s+w}{h+w}\right) + 1.5 + \ln(k)\right] I^2\left(\frac{1}{2} - \frac{\mu_1 d_1}{s}\cos\theta\right)}{m_0 + 2\tau(h-2\Delta h) + \rho sc(h-2\Delta h)} \\ &\quad - \frac{2(\mu_1 F_C + f_2)}{m_0 + 2\tau(h-2\Delta h) + \rho sc(h-2\Delta h)} \end{aligned} \tag{12}$$

When the derivative of the separation, *s,* is calculated from Eq. (12) and equated to zero, the optimal separation at low-frequency can be expressed as:

$$0.2I^2 G_1 M - 0.2I^2 \rho c(h-\Delta h)G_2 - 2\rho c(h-\Delta h)(\mu_1 F_C + f_2) = 0 \tag{13}$$

Where,

$$G_1 = \frac{\mu_1 d_1 \cos\theta}{s^2}\left[2\ln\left(\frac{s+w}{h+w}\right) + 3 + 2\ln(k)\right] + \frac{s - 2\mu_1 d_1 \cos\theta}{s(s+w)}$$

$$G_2 = \ln\left(\frac{s+w}{h+w}\right) + 1.5 + \ln(k) - \frac{\mu_1 d_1 \cos\theta}{s}\left[2\ln\left(\frac{s+w}{h+w}\right) + 3 + 2\ln(k)\right]$$

$$M = m_0 + 2\tau(h-2\Delta h) + \rho sc(h-2\Delta h)$$

The same example case as in Sect. 4.1 is adopted here to illustrate the scenarios at low-frequency conditions. As shown in Fig. 11, when the rail height is set at 14 mm, 18 mm, 22 mm, 26 mm and 30 mm, respectively, the maximum muzzle velocity is 1378.51 m/s, 1148.57 m/s 967.09 m/s, 821.62 m/s and 703.98 m/s, respectively, the separation is 51 mm, 46 mm, 45 mm, 45 mm and 45 mm, respectively, and the corresponding launch load mass is 22.91 g, 26.24 g, 30.04 g, 34.05 g and 38.06 g, respectively. In general, the optimal separation decreases with the increase in the rail height, and the separation is always greater than the rail height, which implies the highest muzzle velocity as generated by a launcher of rectangular calibre.

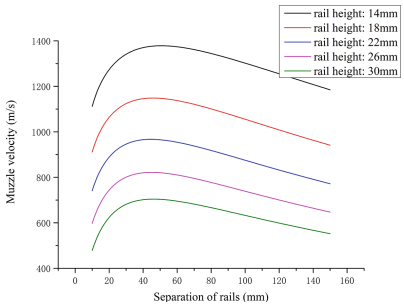

Fig. 11. Variation of muzzle velocity with the separation and height of the rails at low-frequency

From the above calculation results, it can be seen that for high-frequency and low-frequency cases, the variation trend of launch load muzzle velocity with the separation increases first and then decreases, and there is a maximum value. Under the same conditions, the optimal separation at high-frequency is greater than that at low-frequency, and the maximum muzzle velocity at high-frequency is less than that at low-frequency.

5 Conclusions

1) Assuming that the cross-sectional area of the rail is a fixed value, the inductance gradient is the largest when cross section of the rail is rectangular (i.e., width is greater than height) at high-frequency and low-frequency, corresponding to the width-to-height ratio as 3.79 and 3.72, respectively;
2) Under the assumption of pulsed current, both high-frequency and low-frequency muzzle velocities first increase and then decrease with the separation. The optimal separation corresponding to the maximum muzzle velocity decreases with the increase of rail height. The optimal separation at high-frequency is greater than that at low-frequency, and the maximum muzzle velocity at high-frequency is less than that at low-frequency. The maximum muzzle velocity can be obtained for launchers of rectangular calibre (i.e., rail separation is greater than height).

References

1. Li, J., Yan, P., Yuan, W.: Electromagnetic gun technology and its development High Volt. Eng. **40**(04), 1052–1064 (2014). (in Chinese)
2. Ma, W., Lu, J.: Electromagnetic launch technology. J. Nation. Univ. Def. Technol. **38**(06), 1–5 (2016). (in Chinese)
3. Wang, Y., Xiao, F.: The Principle of Electrical Gun. National University of Defense Technology, BeiJing (1995).(in Chinese)
4. McNab, I.R.: Brief history of the EML symposia: 1980–2018. IEEE Trans. Plasma Sci. **47**(5), 2136–2142 (2019). https://doi.org/10.1109/TPS.2018.2885269
5. Kerrisk, J.F.: Current Distribution and Inductance Calculations for Railgun Conductors. Los Alamos National Laboratory, New Mexico, USA (1981)

6. Grover, F.W.: Inductance Calculations: Working Formulas and Tables. Dover Publications, New York (1962)
7. Batteh, J., Powell, J.: Analysis of plasma arcs in arc-driven rail guns. IEEE Trans. Magn. **20**(2), 336–339 (1984)
8. Peng, Z., et al.: Modeling and analysis of time-varying inductance gradient for electromagnetic rail launcher. Trans. China Electrotech. Soc. **35**(23), 4843–4851 (2020). (in Chinese)
9. Xun, R., et al.: Simulation and analysis of electromagnetic field for augmented railgun. High Volt. Eng. **40**(04), 1065–1070 (2014). (in Chinese)
10. Sun, L., Yuan, W., Yan, P.: Study of rail inductance gradient during EM rail launch based on time-frequency analysis. Adv. Technol. Electr. Eng. Energy **27**(02), 38–41 (2008). (in Chinese)
11. Ghassemi, M., Barsi, Y.M., Hamedi, M.H.: Analysis of force distribution acting upon the rails and the armature and prediction of velocity with time in an electromagnetic launcher with new method. IEEE Trans. Magn. **43**(1), 132–136 (2007)
12. Keshtkar, A.: Effect of rail dimension on current distribution and inductance gradient. IEEE Trans. Magn. **41**(1), 383–386 (2005)
13. Keshtkar, A., Bayati, S., Keshtkar, A.: Derivation of a formula for inductance gradient using intelligent estimation method. IEEE Trans. Magn. **45**(1), 305–308 (2009)
14. Li, X., Wang, Z., Wu, H.: Characteristics analysis and optimization design of rail geometry size of electromagnetic railgun. J. Gun Launch Control. **36**(02), 54–58 (2015). (in Chinese)
15. Wang, Z., Yuan, W., Yan, P.: Inductance gradient for rail-type electromagnetic launcher under transient conditions. High Volt. Eng. **43**(12), 4039–4044 (2017). (in Chinese)